Research Article Vol. 11, No. 1 / January 2024 / Optica 1

OPTICA

Low-repetition-rate optical frequency comb

Francesco Canella,[1,2,3,*] Johannes Weitenberg,[2,4] Muhammad Thariq,[2,5] Fabian Schmid,[2,6] Paras Dwivedi,[2,7] Gianluca Galzerano,[3] Theodor W. Hänsch,[2,7] Thomas Udem,[2,7] and Akira Ozawa[2,8]

[1]Dipartimento di Fisica, Politecnico di Milano, Piazza Leonardo da Vinci 32, 20133 Milan, Italy
[2]Max-Planck-Institut für Quantenoptik, Hans-Kopfermann-Straße 1, 85748 Garching, Germany
[3]Istituto di Fotonica e Nanotecnologie–Consiglio Nazionale delle Ricerche, Piazza Leonardo da Vinci 32, 20133 Milan, Italy
[4]Fraunhofer-Institut für Lasertechnik ILT, Steinbachstraße 15, 52074 Aachen, Germany
[5]Karlsruhe School of Optics and Photonics, Karlsruher Institut für Technologie, Schlossplatz 19, 76131 Karlsruhe, Germany
[6]Current address: Institute for Quantum Electronics, ETH Zürich, Otto-Stern-Weg 1, 8093 Zurich, Switzerland
[7]Fakultät für Physik, Ludwig-Maximilians-Universität München, Schellingstraße 4, 80799 Munich, Germany
[8]akira.ozawa@mpq.mpg.de
*francesco.canella@polimi.it

Received 18 September 2023; revised 28 November 2023; accepted 28 November 2023; published 3 January 2024

Reducing the pulse repetition rate of an optical frequency comb increases the pulse energy for a given average power. This enhances the efficiency of nonlinear frequency conversion and it facilitates extending the accessible wavelength range, for example, into the extreme ultraviolet (XUV). The resulting spectrally dense frequency comb can still be used for precision spectroscopy of narrow atomic or molecular transitions. In this paper, we demonstrate a low-noise infrared frequency comb with a repetition rate as low as 40 kHz using a Yb:KYW mode-locked laser, pulse picking, and subsequent amplification. The frequency comb structure is confirmed by generating a beat note with a continuous wave reference laser. A comb mode is actively stabilized to the reference laser, and the integrated rms phase noise from 20 Hz to 20 kHz is measured to be 195 mrad.

https://doi.org/10.1364/OPTICA.506353

1. INTRODUCTION

Optical frequency combs have revolutionized the field of optical frequency metrology [1–3] and are indispensable tools for high-precision laser spectroscopy to study fundamental physics [4–6] and for optical frequency standards [7–11]. The first application of frequency combs was to measure the frequency of a continuous wave laser that is then used for precision spectroscopy [3,12,13]. It is also possible to use the frequency comb itself to excite target transitions and perform spectroscopy with ultra-wide spectral coverage, fast detection times, and high sensitivities [5,14–18].

An optical frequency comb consists of many spectral modes that are equally spaced by the repetition rate of the generating mode-locked pulse train, which is typically in the MHz to the GHz range for conventional solid-state and fiber-laser-based oscillator designs. While combs with mode spacings of several tens of GHz have found applications for calibration of astronomical spectrographs [19,20], a pulse train with a relatively low repetition rate below 10 MHz can have correspondingly higher pulse energy and is therefore advantageous for several applications, including, for example, driving efficient nonlinear processes [21–23]. Nonlinear frequency conversion of optical frequency combs can enable precision spectroscopy in wavelength ranges where continuous wave lasers are not available, such as the extreme ultraviolet (XUV) [24–26]. For example, our planned experiment of precision spectroscopy of the 1S-2S transition in He^+ ions requires an optical frequency comb at 60.8 nm [27,28]. The Ramsey-type frequency comb, which consists of pairs of intense pulses, can be an alternative method to address transitions at XUV wavelengths [29]. Precision spectroscopy of the nuclear transition of ^{229}Th at around 149 nm may find application as a nuclear optical clock [30–33].

Intra-cavity high-order harmonic generation allows the generation of high-power XUV frequency combs suitable for direct frequency comb spectroscopy [24,34–38]. In this scheme, the high-order harmonic generation process is performed inside an enhancement cavity using a gaseous or solid medium placed at the focus of the cavity. Special care must be taken to avoid detrimental effects of the high average power and intensity, such as thermal lensing [39], plasma phase shift [40–42], misalignment due to elevated temperature [39], and damage to the optics [43]. In addition, enhancement cavities for ultrashort pulses have to be carefully designed to tailor the intra-cavity dispersion [44,45].

Alternatively, by operating a comb at a lower repetition rate, a similarly high pulse energy could be achieved with modest average power even without an enhancement cavity. Lowering the repetition rate results in a frequency comb with a smaller mode spacing. For precision spectroscopy, the mode spacing should be at least several times larger than the linewidth of the transition under investigation in order to obtain a comb mode resolved spectroscopy signal. For instance, a signal linewidth of about 1 kHz is expected for the 1S-2S transition in He^+ at 60.8 nm [27,28],

while the nuclear transition of ^{229}Th at about 149 nm has a natural linewidth of about 20 μHz [30,31]. In principle, a comb with a few kHz mode spacing would be sufficient for these applications.

High-pulse-energy ultrafast lasers at such low repetition rates are conventionally generated using master oscillator power amplifiers (MOPAs), where the chirped pulse amplification (CPA) scheme is employed and have found various applications including attosecond physics [46,47], laser particle acceleration [48,49], and ultrafast transient spectroscopy [50]. By actively controlling the round-trip phase shift of the oscillator, each pulse can have an identical carrier–envelope phase (CEP), which is particularly important for the study of field-sensitive phenomena driven by few-cycle pulses [51]. Using the balanced optical cross-correlator method [52], the pulse-to-pulse timing jitter of the CPA laser system can be controlled precisely. For example, in Ref. [53] a sub-100 fs timing jitter is demonstrated at 1 kHz repetition rate. A pulse timing jitter of 100 fs still introduces a relative frequency uncertainty of 10^{-10} at a repetition rate of 1 kHz. This corresponds to a broadening of the optical comb modes that is larger than the mode spacing and could wash out the comb structure in the frequency domain. Although such CEP-stabilized low-repetition-rate laser systems have been shown to be suitable for studying ultrafast phenomena, they do not guarantee a low-noise frequency comb structure.

In this work, we report a low-noise optical frequency comb that operates at tunable repetition rates from 40 kHz to 40 MHz using a Yb:KYW mode-locked oscillator. Mode-locked lasers oscillating directly at sub-MHz repetition rates would require very long cavities, which may not be practical. Instead, conventional mode-locked lasers and pulse pickers are used to generate optical frequency combs at low repetition rates [54,55]. The associated power loss is compensated for by re-amplifying the pulse train such that higher pulse energy is achieved. A comb mode is actively stabilized to an ultra-stable continuous wave (cw) reference laser. The phase noise of the stabilized mode is characterized with respect to the reference laser and is shown to result in a narrow linewidth suitable for exciting narrow transitions.

2. MODELING OF THE PULSE PICKING PROCESS

In this section, we first model the pulse picking process by treating the pulse picker as an ideal amplitude modulator.

For mathematical convenience, we model the output of the mode-locked laser as a train of Gaussian-shaped pulses with a repetition rate f_{rep}. The temporal pulse spacing is $T = f_{\mathrm{rep}}^{-1}$. The electric field $E(t)$ of the laser pulse train can be described as

$$E(t) = A \sum_{k=-\infty}^{\infty} \exp\left[-\frac{(t-kT)^2}{\Delta t^2}\right] e^{i(\omega_0 t+\varphi(t))}, \tag{1}$$

where A is the field envelope peak amplitude, ω_0 is the angular frequency of the carrier, and Δt is the pulse duration defined by the $1/e$ half-width of the field amplitude. The residual phase fluctuation after comb stabilization is represented by $\varphi(t)$. For simplicity, the CEO frequency of the comb is assumed to be zero in Eq. (1) by assuming that the carrier frequency ω_0 is an integer multiple of the pulse repetition rate $2\pi/T$. Including a finite CEO frequency in the calculation is straightforward, and does not change the results. We introduce pulse picking by assuming that the laser pulses pass through an ideal amplitude modulator with a rectangular-shaped gating that selects every m-th pulse. We call m the pulse picking factor. The pulse picker reduces the average power and the repetition rate by a factor m and hence the power in each of the modes by a factor m^2. Under the approximation that the electric field amplitude at the rising and falling edges of the rectangular-shaped gating is negligible, the pulse-picked field $E_p(t)$ can be written as

$$\begin{aligned} E_{\mathrm{p}}(t) &= A \sum_{k=-\infty}^{\infty} \exp\left[-\frac{(t-mkT)^2}{\Delta t^2}\right] e^{i(\omega_0 t+\varphi(t))} \\ &\equiv E_{\mathrm{p},0}(t) e^{i\varphi(t)}, \end{aligned} \tag{2}$$

where $E_{\mathrm{p},0}(t)$ is defined as the noiseless component of the pulse-picked field. The spectrum of the pulse-picked field $E_{\mathrm{p}}(t)$ is given by

$$\tilde{E}_{\mathrm{p}}(\omega) = \int_{-\infty}^{\infty} E_{\mathrm{p}}(t) e^{-i\omega t} \mathrm{d}t \approx \tilde{E}_{\mathrm{p},0}(\omega) + \frac{i}{2\pi}\left(\tilde{E}_{\mathrm{p},0} * \tilde{\varphi}\right)(\omega), \tag{3}$$

where the approximation is valid for small rms phase noise with a vanishing mean, i.e., $e^{i\varphi(t)} \approx 1 + i\varphi(t)$. In Eq. (3), the convolution is defined as $(\tilde{E}_{\mathrm{p},0} * \tilde{\varphi})(\omega) = \int_{-\infty}^{\infty} \tilde{E}_{\mathrm{p},0}(\omega')\tilde{\varphi}(\omega-\omega')\mathrm{d}\omega'$, where $\tilde{E}_{\mathrm{p},0}(\omega)$ and $\tilde{\varphi}(\omega)$ are Fourier transforms of $E_{\mathrm{p},0}(t)$ and $\varphi(t)$, respectively. The main Fourier components of $\tilde{E}_{\mathrm{p},0}(\omega)$ and $\tilde{\varphi}(\omega)$ are in the optical and the radio frequency domain, respectively. The spectrum of the noiseless component is given by

$$\begin{aligned} \tilde{E}_{\mathrm{p},0}(\omega) &= A \int_{-\infty}^{\infty} \sum_{k=-\infty}^{\infty} \exp\left[-\frac{(t-mkT)^2}{\Delta t^2}\right] e^{i(\omega_0-\omega)t} \mathrm{d}t \\ &= \frac{2\pi^{3/2}\Delta t}{mT} A \exp\left[-\frac{1}{4}\Delta t^2(\omega-\omega_0)^2\right] \\ &\quad \times \sum_{n=-\infty}^{\infty} \delta\left(\omega - \frac{2\pi n}{mT}\right). \end{aligned} \tag{4}$$

As expected, the spectrum after pulse picking consists of comb modes with a mode spacing of $1/mT = f_{\mathrm{rep}}/m$, as expressed by the sum over the delta functions $\delta(\omega - 2\pi n/mT)$. The newly created comb modes can be considered as the sidebands at subharmonics of the original repetition rate introduced by the amplitude modulation that selects every m-th pulse (see Supplement 1 for a detailed derivation). These additional sidebands fill in the gaps between the modes of the original comb. The Gaussian spectral envelope is maintained also for the newly added modes since the picked pulses are still Gaussian in the time domain.

The spectral intensity can be calculated as $\tilde{I}_{\mathrm{p},0}(\omega) \propto |\tilde{E}_{\mathrm{p},0}(\omega)|^2$ demonstrating that the comb mode power scales with m^{-2} as explained above. Note that $|\tilde{E}_{\mathrm{p},0}(\omega)|^2$ includes the squares of the delta functions, i.e., infinite power density at the frequencies of the modes compatible with an infinite number of pulses. Using Eq. (4) in the last term of Eq. (3), we find that the phase noise is convolved into all comb modes, including the new modes created by pulse picking. The phase noise spectrum $\tilde{\varphi}(\omega)$ for radio frequencies $|\omega| > 2\pi/mT$ is folded into $|\omega| < 2\pi/mT$. In the time domain, the effect can be considered as an aliasing where the phase noise at $|\omega| > 2\pi/mT$ is undersampled by the pulse train. If the phase noise spectrum $\tilde{\varphi}(\omega)$ is flat and extends up to the original repetition rate, reducing the repetition rate by a factor of m will result in

an m-fold increase in the power spectral density (PSD) of the phase noise in the frequency range of $|\omega| < 2\pi/mT$. On the other hand, the integrated phase noise does not change after pulse picking because the m-fold increase in the PSD is canceled by an inverse reduction of the maximum frequency, i.e., the Nyquist frequency reduces by a factor m. This is consistent with Eqs. (1) and (2), which contain identical noise terms $e^{i\varphi(t)}$, and the rms phase noise is expected to be identical before and after pulse picking.

The model described here shows that the phase noise already present in the original pulse train affects the frequency comb structure equally before and after pulse picking, regardless of the repetition rate. A trivial requirement is that the linewidth of the comb modes prior to pulse picking should be narrower than the mode spacing after pulse picking to avoid washing out the comb structure. In addition, the actual implementation of the pulse picker and the subsequent amplification should be low-noise to preserve the comb structure at lower repetition rates. Our work described in Sections 3 and 4 aims to experimentally confirm that this is possible.

Pulse picking can be implemented using an acousto-optical modulator (AOM) or a combination of an electro-optic modulator (EOM) and a polarizer. In Fig. 1, we show a conceptual scheme of an AOM-based pulse picking. The AOM is driven at a carrier frequency f_{AOM} (typically tens or hundreds of MHz) that is amplitude modulated with gating pulses. Here we assume a rectangular-shaped gate function with repetition rate f_{gate} (time spacing $T_{\mathrm{gate}} = f_{\mathrm{gate}}^{-1}$) and a width of τ. In Supplement 1, we discuss the effect of gating timing jitter. The RF drive signal for the AOM can be described as

$$V_{\mathrm{RF}}(t) = \sum_{n=-\infty}^{\infty} A_{\mathrm{RF}}\left(t - nT_{\mathrm{gate}}\right) e^{i\omega_{\mathrm{AOM}}t}, \tag{5}$$

where A_{RF} is the rectangular-shaped gate function, and $\omega_{\mathrm{AOM}} = 2\pi f_{\mathrm{AOM}}$.

The modulator diffracts every m-th pulse to the first diffraction order, and the rest is sent to a beam dump. The Fourier transform of Eq. (5) shows that the spectrum of the RF signal consists of narrow lines spaced by f_{gate}, similar to an optical frequency comb. The frequency of the RF modes is given by

$$f_{\mathrm{RF},n'} = n' f_{\mathrm{gate}} + f_{\mathrm{AOM}}, \tag{6}$$

with an integer n'. The frequency of the optical comb modes $f_{n,n'}$ after pulse picking is given by the sum of the original comb mode frequencies and the AOM RF frequencies:

$$\begin{aligned} f_{n,n'} &= n f_{\mathrm{rep}} + f_{\mathrm{CEO}} + f_{\mathrm{RF},n'} \\ &= n f_{\mathrm{rep}} + n' f_{\mathrm{gate}} + f_{\mathrm{CEO}} + f_{\mathrm{AOM}}, \end{aligned} \tag{7}$$

where f_{CEO} is the CEO frequency of the original comb. To obtain an equidistant comb structure after pulse picking, the ratio $f_{\mathrm{rep}}/f_{\mathrm{gate}}$ must be an integer. In the time domain, this condition translates to the requirement that $T_{\mathrm{gate}} = mT$, with m introduced in Eq. (2). The CEO of the pulse-picked comb remains unchanged after pulse picking if $f_{\mathrm{AOM}}/f_{\mathrm{gate}} = q$ is an integer. With an integer q, we can define a new mode-index $\tilde{n} \equiv n' + q + nm$ to find a compact expression for the mode frequencies of the pulse-picked comb:

$$f_{\tilde{n}} = \tilde{n}\frac{f_{\mathrm{rep}}}{m} + f_{\mathrm{CEO}}. \tag{8}$$

In the special case of zero CEO frequency ($f_{\mathrm{CEO}} = 0$), a pulse train with a constant CEP can be obtained, which finds interesting applications in attosecond physics [56–58].

3. EXPERIMENT

Figure 2 shows our setup for generating and testing a low-repetition-rate optical frequency comb. A home-built Yb:KYW oscillator is mode-locked by soft-aperture Kerr-lensing and generates a 40 MHz pulse train. The output spectrum is centered at 1030 nm and has an FWHM bandwidth of 14 nm. The average output power is 26 mW. The FWHM temporal pulse duration is measured to be 89 fs using the intensity autocorrelation method (autocorrelation length 137 fs), assuming sech^2 pulse shape.

Two PZT-actuated mirrors are installed in the laser cavity to control the cavity length and are used to stabilize the frequency comb (PZT stands for lead zirconate titanate). One such mirror is a high-reflectivity mirror fixed to a PZT (Thorlabs PA4DGW) that is mounted on a high-damping alloy and has a bandwidth of about 10 kHz. The other mirror is the laser output coupler, which is actuated by a linear stage (Newport 9066-X-V-M) driven by a PZT actuator (Thorlabs PK2FVF1). This second PZT-actuated mirror is used to compensate for slow drifts. The laser cavity is placed on

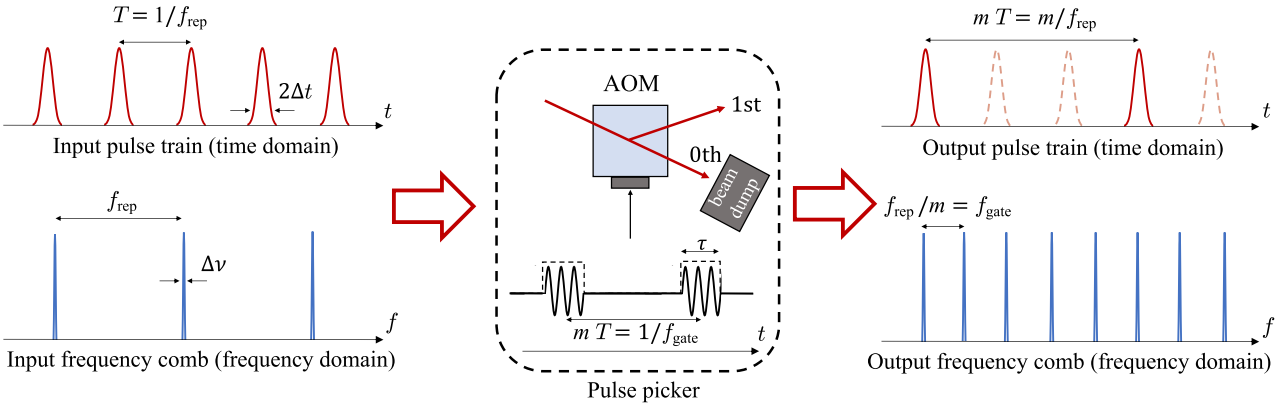

Fig. 1. Low-repetition-rate frequency comb generation using an AOM-based pulse picker. Every m-th pulse is diffracted by the AOM to the first diffraction order, while the others remain in the zeroth order and are dumped. After the pulse picking, the pulse-to-pulse time interval increases by the factor m, while the mode spacing in the frequency domain becomes m times smaller. The AOM is driven by an RF carrier that is amplitude modulated with a rectangular-shaped gate-pulse train.

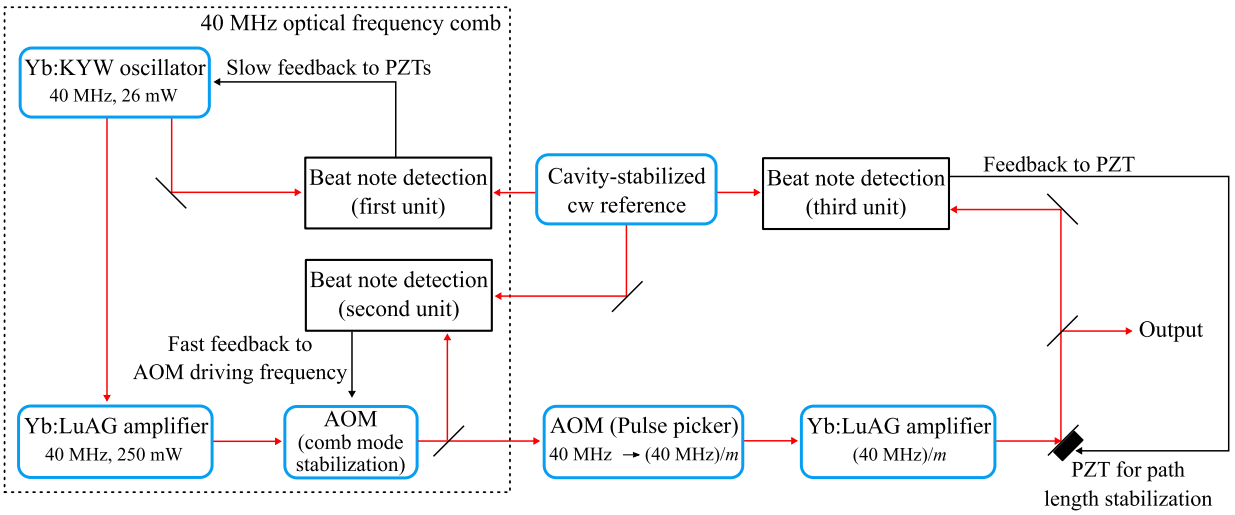

Fig. 2. Schematic of the experimental setup. The 40 MHz optical frequency comb (dotted box) consists of a mode-locked Yb:KYW oscillator, a solid-state amplifier using Yb:LuAG as a gain medium, and an AOM frequency shifter for fast control of the stabilized comb mode frequency. Slower control acts on PZT-actuated mirrors of the laser cavity (PZTs). The output of the Yb:KYW oscillator is centered at 1030 nm with a bandwidth of 14 nm. The error signal for phase stabilization of one of the comb modes is obtained from beat notes between that mode and an ultra-stable cw reference laser emitting at 1033 nm. The cw reference laser is amplified by a semiconductor optical amplifier (BOA1050P Thorlabs, not shown) before sending it to the second and third beat note detection units. An AOM-based pulse picker reduces the comb's repetition rate to $(40\ \mathrm{MHz})/m$, where m is the pulse picking factor. After the pulse picker, the pulses are re-amplified by a second Yb:LuAG amplifier. The third feedback loop controls a PZT-actuated mirror in the beamline and reduces the phase noise due to fluctuations in the beam path length.

a vibration-isolated, temperature-stabilized aluminum baseplate and installed inside an air-tight aluminum housing [59].

At the laser output, the repetition rate f_{rep} is detected with a fast photodiode (Thorlabs DET01CFC, not shown in Fig. 2). The laser has an auxiliary output that is taken from the reflection of an intracavity optic element with a compromised spectral phase compared with the main output. This second output has about 60 mW of power and is sent into a heterodyne beat detection setup with a continuous wave (cw) reference laser. The cw reference laser operates at 1033 nm and is stabilized to an ultra-stable reference cavity. The rms phase noise of the reference laser was measured to be 10.2 mrad integrated from 10 kHz to 10 MHz with respect to the reference cavity [60].

In the heterodyne beat detection setup, about 100 comb modes are filtered out around the frequency of the cw reference laser using an interference filter (Alluxa A4017) and an etalon (LightMachinery OP-6204-M, 7.3 GHz FWHM bandwidth). The beat signal between the frequency comb and the reference laser is detected using balanced photodetectors (Koheron PD100B), which suppresses the contribution of classical amplitude noise [61]. The RF beat signal is filtered to isolate the beat note between the closest comb modes and the reference laser. Then the signal is phase-compared to a 10 MHz signal generated by a signal generator (Marconi Instruments 2022C). The signal controls the PZT actuators of the Yb:KYW laser via a home-built loop filter. This way, one of the comb modes is phase-stabilized to the cw reference laser.

The frequency comb is amplified by a solid-state double-pass Yb:LuAG amplifier pumped by a multimode diode laser operating at around 935 nm. With an input seed power of 26 mW, we obtain 250 mW at the output when the pump power is set to 7.2 W. Since the gain bandwidth of Yb:LuAG is about 5 nm [62,63], a significant gain narrowing effect reduces the bandwidth of the amplifier output to 2.7 nm. The peak gain at 1030 nm is approximately 16.6 dB. The amplifier output is sent to an AOM (AA Opto Electronic MT110) that is used to stabilize one of the comb modes in combination with the PZTs in the laser cavity. The first-order diffraction of the AOM downshifts the entire frequency comb of the laser by about 110 MHz. The diffraction efficiency of the AOM is about 70%. The second beat signal between the frequency comb and the reference cw laser is obtained after the AOM. The beat signal is compared with the 10 MHz frequency reference and is sent to a loop filter (Vescent Photonics D2-125). The loop filter's output is sent to a voltage-controlled oscillator (VCO, Pasternack Enterprises Inc. PE1V31008), which generates the RF signal that drives the AOM. The control bandwidth is estimated to be >100 kHz, limited by the time required for the acoustic wave inside the AOM to reach the laser beam. In principle, it would be possible to control the slow feedback using the error signal obtained from the second beat detection unit, thus eliminating the first beat detection unit. We find our scheme technically convenient because the accidental failure of the second feedback does not affect the first one.

The following pulse picker AOM (AA Opto Electronic MT200-A0.4-1064) is driven at a carrier frequency of $f_{\mathrm{AOM}} = 200$ MHz. It selects every m-th pulse by amplitude modulating the carrier with a rectangular-shaped envelope. A rectangular gate signal with a pulse width of $\tau = 32$ ns at a frequency of $f_{\mathrm{gate}} = f_{\mathrm{rep}}/m$ is used. The gate pulse width is less than $2T$ as required to select individual pulses. An RF switch (Minicircuit ZASWA-2-50DR+) is used for the modulation. The diffraction efficiency of the AOM is measured to be $>60\%$, and the pulses remaining in the zeroth order are sent to a beam dump. The gate signal is generated by a delay generator (Alphanov Tombak) using the repetition rate signal from the Yb:KYW oscillator as the timing source. The RF carrier signal to drive the AOM is derived from the fifth harmonic of the repetition rate, which is generated in the detection with a high-bandwidth photodiode. A band-pass

filter with a 3 dB bandwidth of 10 MHz is used to isolate the fifth harmonic. In this way, the gate signal, the repetition rate, and the AOM RF carrier are phase synchronized. The RF switch produces a modulation with 10%–90% rise/fall times of 5 ns. Measuring the energy of the picked pulses for different gating delays with respect to the pulses reveals the time response of the AOM. The 10%–90% rise and fall time of the AOM was measured to be 7.5 ns. This is dominated by the time it takes for the acoustic wave to cross the focused laser beam at the point of interaction. From the speed of sound within the modulator material (TeO_2) of 4200 m/s and the laser beam diameter of $2w_0 = 39$ µm, the rise/fall time is estimated to 6 ns.

The picked pulses are sent to a second Yb:LuAG amplifier that is similar in design to the first amplifier. When the pump power is set to 14 W, the amplifier output power is 2. 5 W, 374 mW, 43 mW, and 8 mW at a repetition rate of 40 MHz, 4 MHz, 400 kHz, and 40 kHz, respectively. The output pulse train of the second amplifier is measured by a fast InGaAs photodiode (Thorlabs DET01CFC, 1.2 GHz bandwidth) and a 2.5 GHz oscilloscope (LeCroy WavePro 7Zi). The results are shown in Fig. 3 at repetition rates of 40 MHz, 4 MHz, 400 kHz, and 40 kHz.

We find that the pulse-picked beam still contains a tiny fraction of the pulse train at the original repetition rate of 40 MHz. This is not due to incomplete suppression of the RF carrier, but is caused by scattering within the AOM material. We could suppress the optical power of this component by 28 dB compared to the picked pulses. This was achieved by carefully adjusting the size and position of an iris surrounding the pulse-picked laser beam.

A PZT-actuated mirror is introduced in the beamline after the second amplifier to compensate for possible low-frequency phase fluctuations due to free-space parts of the setup, e.g., mirrors or breadboard vibrations. In addition, the phase noise introduced by the pulse picker and amplifier is partially compensated for. A portion of the beam after the PZT actuated mirror is sent to the third beat detection setup. The beat signal is then phase compared to a reference at 11.3 MHz from an electronic synthesizer (Marconi Instruments 2022C) and is used as an error signal to drive the PZT via a home-built loop filter. The in-loop error signal shows a peak at about 4 kHz when the feedback gain is too high, indicating a control bandwidth of approximately 4 kHz. This is fast enough to significantly suppress low-frequency phase noise caused by mechanical and acoustic vibrations. Supplement 1 shows a comparison of the beat note spectra with path length stabilization on and off.

4. RESULTS AND DISCUSSION

The evaluated beat note spectra are obtained from the third beat note detection unit (Fig. 2) and shown in Fig. 4. The acquisitions were made at repetition rates of 40 MHz (no pulse picking), 4 MHz, 400 kHz, and 40 kHz with resolution bandwidths of 10 kHz, 1 kHz, 100 Hz, and 10 Hz, respectively. A clear comb structure is maintained even at the reduced repetition rate of

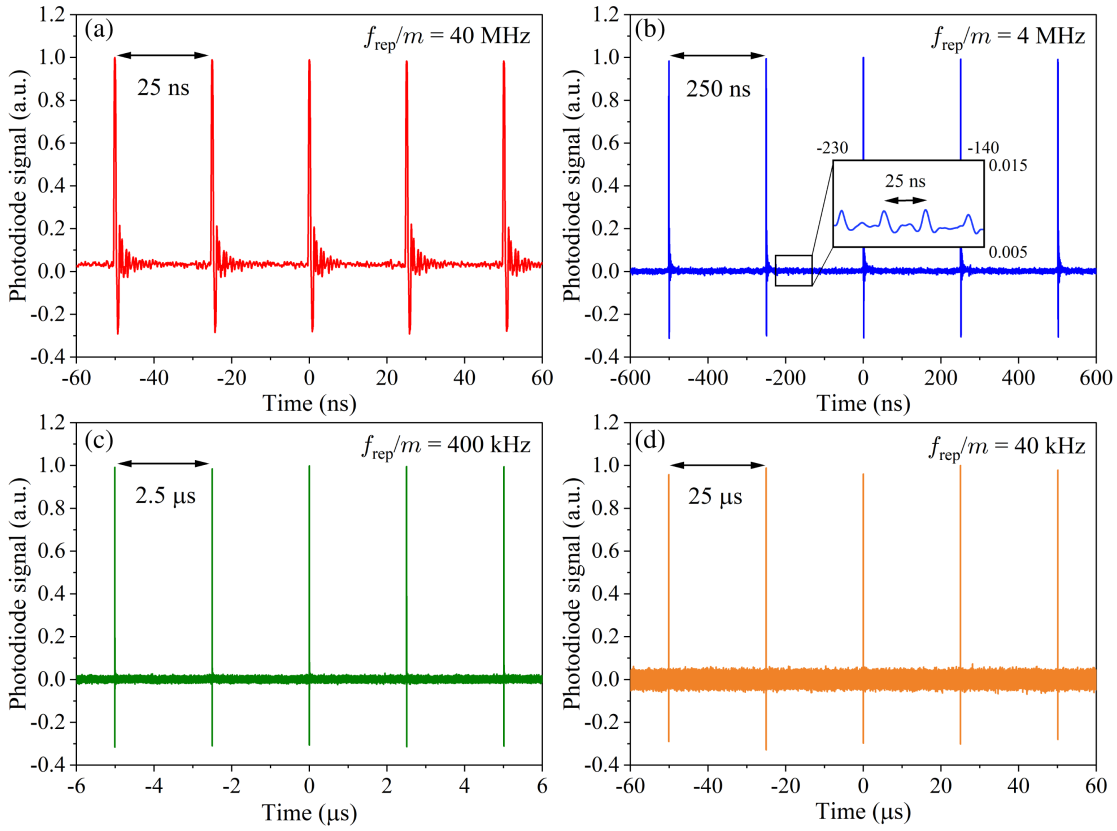

Fig. 3. Time domain traces of pulses after pulse picking and the second amplifier ("Output" in Fig. 2). The negative signal is due to ringing. (a) At a repetition rate of 40 MHz without pulse picking ($m = 1$). (b) At a repetition rate of 4 MHz, which corresponds to a pulse-to-pulse interval of 250 ns and a pulse picking factor of $m = 10$. The magnified inset shows a trace averaged over 1000 acquisitions where residual 40 MHz pulses are visible with about 28 dB of suppression. (c) Pulses at a repetition rate of 400 kHz, corresponding to $m = 10^2$ (2.5 µs pulse-to-pulse interval). (d) Pulses at 40 kHz repetition rate, corresponding to a pulse-to-pulse interval of 25 µs and $m = 10^3$. The oscilloscope sampling rate is 40 Gs/s for all traces.

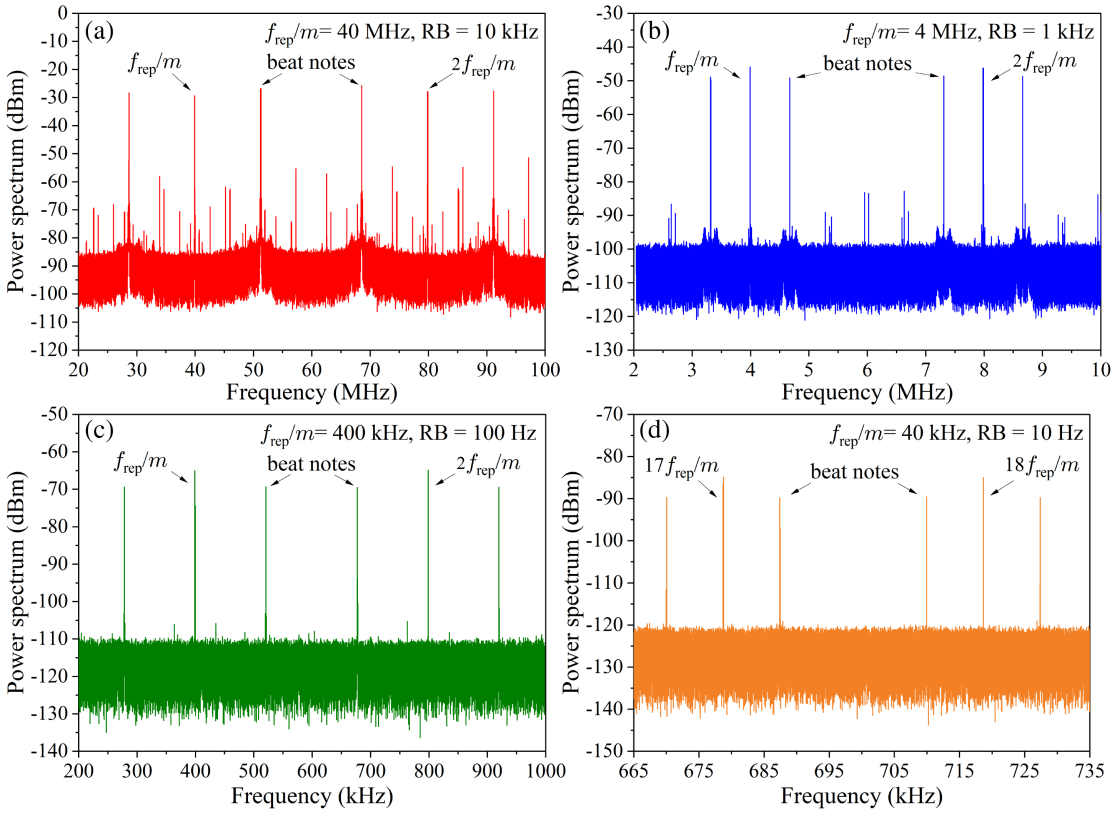

Fig. 4. Beat note spectra acquired from the third beat note detection unit at different repetition rates of (a) 40 MHz, (b) 4 MHz, (c) 400 kHz, and (d) 40 kHz. A resolution bandwidth (RB) of 10 kHz, 1 kHz, 100 Hz, and 10 Hz was used, respectively. In all plots except for (d), two peaks that correspond to f_{rep}/m and $2f_{rep}/m$ are visible in addition to two peaks that correspond to the beat frequencies. The repetition rate signal is strongly suppressed by balanced photodetection. The trace acquired for 40 kHz shows frequencies between the 17th and the 18th harmonics of f_{rep} to avoid the elevated noise floor of the measurement setup at low frequencies. The RF spectrum at 40 MHz repetition rate without pulse picking shown in (a) contains several peaks between the repetition rate peaks and the beat notes. Most of these are due to the mixing of the strong repetition rate and beat note signals on the photodiode.

40 kHz, where a narrow beat note peak is still visible with a signal-to-noise ratio above 30 dB. For all repetition rates, the linewidth of the beat signal is limited by the resolution bandwidth of the spectrum analyzer (Agilent E4445A).

Figure 5 shows the RF power of the beat notes for different pulse picking factors m. The electrical beat note power is proportional to the optical power contained in a single comb mode and scales with $1/m^2$, as expected from the spectral intensity $I_{p,0}(\omega)$ of our model in Eq. (4).

The power spectral density (PSD) of the phase noise is obtained by Fourier transforming the recorded time trace, assuming that $\varphi(t)$ is small. Analyzing the heterodyne beat note allows to bring optical phase noise to the RF domain, where it can be recorded and analyzed. In a sense, the convolution of Eq. (3) converts the RF noise of $\tilde{\varphi}(\omega)$ into the optical domain, while heterodyning brings it back into the RF domain. The time traces contain 2.05×10^8 samples, and the Blackman window was applied before performing the Fourier transform to minimize the contribution of sidelobes. The sideband spectrum of the Fourier transform trace around the beat frequency gives the PSD of the phase noise after normalization to the peak amplitude of the beat note. Since the beat signal becomes weaker when lowering the repetition rate of the comb, the phase noise PSD experiences a relative increase in the noise floor. To overcome this issue, the gated optical noise reduction (GATOR) technique described by Deschênes and Genest in Ref. [64] was used to evaluate the data. In the time domain, the beat note of a

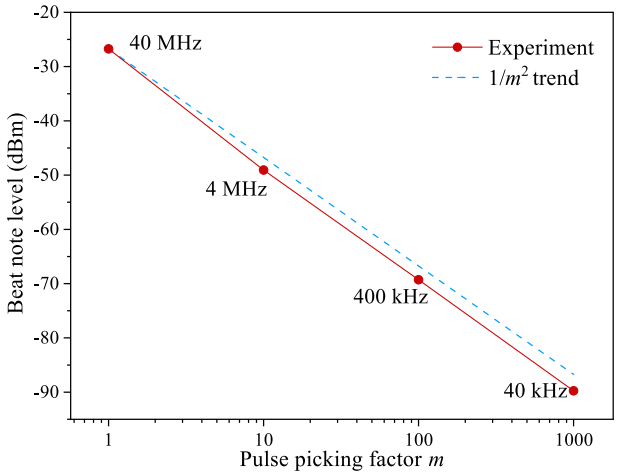

Fig. 5. Beat note power level as a function of the pulse picking factor m. The dashed line shows a trend proportional to m^{-2}, as expected from the pulse picking model. The trend line is drawn assuming the 40 MHz point as reference.

frequency comb with a cw laser can be understood as the pulse train sampling the cw wave, i.e., the beat note signal is available only for the duration of the pulses. The GATOR technique strongly suppresses the noise from the cw reference laser and the detection setup by evaluating the beat signal only within narrow time windows

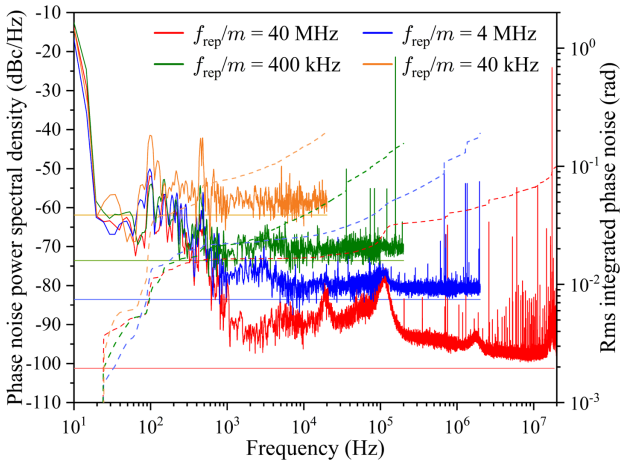

Fig. 6. Power spectral density (PSD) of phase noise at different repetition rates obtained by the GATOR technique (solid traces). Straight horizontal lines indicate the average of the noise floor of the measurement (only cw reference processed in the same way as the beat signal) for each PSD trace. The rms integrated phase noise is also shown (dashed lines). The endpoint of the integration is at the Nyquist frequency, i.e., $f_{rep}/2m$. Higher-frequency-noise contributions are aliased such that the endpoints of the dashed lines give the total phase noise. These endpoints are comparable for all the picked pulse trains. The strong peak at about 20 MHz on the 40 MHz repetition rate trace is due to a neighboring beat note.

around the comb pulses. In the frequency domain, the GATOR method effectively averages the spectrum of the beat notes between the cw laser and several different comb modes. This increases the signal-to-noise ratio compared to beat detection with a single comb mode. We used a software implementation of GATOR by introducing temporal gate windows around each of the pulses. The width of the gate windows was set to 40 ns for all repetition rates, limited by the bandwidth of the detector. The resulting phase noise PSDs are shown with solid lines in Fig. 6. To evaluate the noise floor, we repeated the same measurement without comb pulses and reperformed the same analysis. Since for traces in which the pulse separation time is lower than the gate window width the GATOR does not affect the data, we used for simplicity the ungated data to compute the 40 MHz of Fig. 6.

The PSD of the original frequency comb at 40 MHz repetition rate contains low-frequency phase noise up to about 1 kHz due to uncompensated environmental vibrations. Two broad noise peaks at about 20 kHz and 100 kHz are servo bumps from feedback loops controlling the fast PZT actuator in the laser cavity and the AOM used for phase stabilization, respectively. The servo bump of the PZT for path length stabilization is around 400 Hz. The peak at 17.3 MHz in the 40 MHz trace is due to the neighboring beat note. Other spurious signals that we attribute to radio frequency pickups are visible at frequencies beyond 100 kHz. The noise floor is determined by the amplitude noise of the cw reference laser, the noise of the photodetectors, and the electronics used in the beat detection setup. It increases for lower repetition rates due to reduced carrier power of the beat signal. The low-frequency noise below 1 kHz is the same for repetition rates of 40 MHz, 4 MHz, and 400 kHz. At a repetition rate of 40 kHz, some of the noise structure below 1 kHz appears 5–10 dB higher than other repetition rates, which contributes to the increase of the rms integrated phase noise of about 50 mrad. This might be due to the different gain settings of the path length stabilization feedback to compensate for the different beat note power levels for various repetition rates. No other significant increase in phase noise was observed above the noise floor for the pulse-picked frequency combs. The FWHM linewidth of the frequency comb is limited by the resolution bandwidth of the measurement (10 Hz) for all repetition rates investigated.

The rms phase noise integrated from 20 Hz to half the repetition rate $f_{rep}/2m$ was calculated from the PSD spectra. They are 100 mrad, 190 mrad, 156 mrad, and 195 mrad for repetition rates of 40 MHz, 4 MHz, 400 kHz, and 40 kHz, respectively. The contributions of the harmonic peaks of f_{rep} and the beat notes are not representing the phase noise of the comb mode and are therefore excluded from the integration. For all repetition rates, the measurement noise floor contributes significantly to the rms integrated phase noise. Therefore, our measurement gives the upper limit of the phase noise of the pulse-picked comb.

The measurements presented here are based on in-loop signals. In our case, this is sufficient to determine the noise of the low-repetition-rate laser relative to the cw reference laser. The phase noise is not less than the measurement noise floor at any frequency. Therefore, our in-loop phase noise measurement adequately reflects the upper limit of the phase noise of our low-repetition-rate laser system relative to the cw reference laser. Note that the path length stabilization used here should be implemented in any application of the low-repetition-rate frequency comb.

It is interesting to consider what limits the lowest possible repetition rate. In the laser system discussed here, the high-repetition-rate frequency comb is stabilized before pulse picking using a method described in Section 3. The amplifier setup after pulse picking is prone to additional noise and more difficult to actively stabilize. This is because the error signal for path length stabilization is taken from low-repetition-rate pulses and the available feedback bandwidth is limited to half the repetition rate. In the time domain, the servo system needs to receive at least two pulses before it can know if the phase shift has changed. As a result, the phase noise at Fourier frequencies significantly lower than half the repetition rate can be efficiently suppressed, while noise at higher frequencies remains unsuppressed. Note that feedback systems based on proportional–integral–differential (PID) controllers require their control bandwidth to be much larger than the frequency of the noise in order to achieve a small phase delay that allows high feedback gain at lower frequencies while suppressing oscillation at higher frequencies [65]. The amazing accuracy of optical frequency combs comes from their steady-state operation, i.e., a regular pulse train that finds the same environment for each pulse. Steady-state operation is disturbed when the pulse-to-pulse interval is longer than the typical time scale of the phase noise introduced by the environment, and the disturbance cannot be actively stabilized due to limited feedback bandwidth. This problem is significant for repetition rates below 10 kHz where acoustic vibrations of many standard optical components are significant. The lowest possible repetition rate depends on the type of amplifier and the design of the setup. Our amplifiers are pumped with a cw pump source and therefore pulse-to-pulse phase variations are minimized. It also does not rely on the CPA scheme, which can introduce wavelength-dependent phase fluctuations. Our demonstration shows that the compact and simple solid-state amplifiers used here introduce sufficiently low phase noise to maintain the comb structure at a repetition rate as low as 40 kHz.

To increase the feedback bandwidth significantly beyond the repetition rate after pulse picking, a probe laser with a higher

repetition rate or even a continuous wave laser could be superimposed on the beamline to monitor the phase variations. However, we expect limitations of this method because the probe beam would have a different peak intensity and spectrum. Intensity and spectrum-dependent phase shifts expected in an optical amplifier, pulse compressor, and nonlinear frequency conversion cannot be easily accounted for in this way.

5. CONCLUSIONS AND FUTURE PROSPECTS

In this paper, we have demonstrated a low-repetition-rate optical frequency comb based on a Yb:KYW solid-state mode-locked oscillator using an AOM pulse picker. The repetition rate is adjustable over three orders of magnitude from 40 MHz to 40 kHz. One of the modes of the frequency comb is tightly phase-locked to a cavity-stabilized ultra-low-noise cw laser by measuring the heterodyne beat note between them and providing feedback to the cavity length of the oscillator, an external AOM, and a PZT actuated mirror in the beamline. We have characterized the phase noise of the frequency comb at repetition rates of 40 MHz, 4 MHz, 400 kHz, and 40 kHz with respect to the reference cw laser. The results confirm that a narrow linewidth comb structure is preserved even after pulse picking. Using the power spectral density of the phase noise obtained using the GATOR technique, the integrated rms phase noise was evaluated to be 195 mrad at 40 kHz repetition rate. For the first time, to the best of our knowledge, we demonstrate optically stabilized low-noise frequency combs at repetition rates as low as a few tens of kHz.

The pulse energy and average power were 200 nJ and 8 mW at a repetition rate of 40 kHz. A solid-state amplifier similar to the one used in this work can be added to increase the pulse energy to a >10 μJ level. Frequency combs with such high pulse energy and moderate average power are expected to be useful for driving high-order harmonic generation processes and generating XUV frequency combs [66]. The low-noise and narrow linewidth comb modes shown here indicate that low-repetition-rate frequency combs are a promising option for high-resolution spectroscopy at exotic wavelengths. Dual comb spectroscopy at XUV wavelengths can be an interesting application of the low-repetition-rate XUV frequency combs.

When direct frequency comb spectroscopy is performed using frequency combs with a low repetition rate, it may be difficult to determine the comb mode number. If the pulse picking factor is large and the uncertainty of the line center determination is small enough, the comb mode number can be unambiguously determined by repeating the measurement for different pulse picking factors.

The single-pass pulse picking scheme used in this study is inefficient for reducing the repetition rate because most of the original pulses are unused. In the future, we plan to perform pulse picking in a femtosecond buildup cavity to avoid the loss of average power [67,68]. Intracavity pulse picking will also serve as a narrow spectral filter to efficiently suppress phase and amplitude noise at frequencies greater than half the resonance width.

Funding. European Research Council (742247).

Acknowledgment. T.W. Hänsch acknowledges support from the Max-Planck Foundation.

Disclosures. The authors declare no conflicts of interest.

Data availability. Data supporting the results presented in this paper are available from the authors upon reasonable request.

Supplemental document. See Supplement 1 for supporting content.

REFERENCES

1. T. Udem, R. Holzwarth, and T. W. Hänsch, "Optical frequency metrology," Nature **416**, 233–237 (2002).
2. D. J. Jones, S. A. Diddams, J. K. Ranka, *et al.*, "Carrier-envelope phase control of femtosecond mode-locked lasers and direct optical frequency synthesis," Science **288**, 635–639 (2000).
3. S. A. Diddams, K. Vahala, and T. Udem, "Optical frequency combs: coherently uniting the electromagnetic spectrum," Science **369**, eaay3676 (2020).
4. A. Beyer, L. Maisenbacher, A. Matveev, *et al.*, "The Rydberg constant and proton size from atomic hydrogen," Science **358**, 79–85 (2017).
5. A. Grinin, A. Matveev, D. C. Yost, *et al.*, "Two-photon frequency comb spectroscopy of atomic hydrogen," Science **370**, 1061–1066 (2020).
6. S. Patra, M. Germann, J.-P. Karr, *et al.*, "Proton-electron mass ratio from laser spectroscopy of HD^+ at the part-per-trillion level," Science **369**, 1238–1241 (2020).
7. S. A. Diddams, T. Udem, J. C. Bergquist, *et al.*, "An optical clock based on a single trapped $^{199}Hg^+$ ion," Science **293**, 825–828 (2001).
8. B. J. Bloom, T. L. Nicholson, J. R. Williams, *et al.*, "An optical lattice clock with accuracy and stability at the 10^{-18} level," Nature **506**, 71–75 (2014).
9. I. Ushijima, M. Takamoto, M. Das, *et al.*, "Cryogenic optical lattice clocks," Nat. Photonics **9**, 185–189 (2015).
10. M. Schioppo, R. C. Brown, W. F. McGrew, *et al.*, "Ultrastable optical clock with two cold-atom ensembles," Nat. Photonics **11**, 48–52 (2017).
11. S. M. Brewer, J.-S. Chen, A. M. Hankin, *et al.*, "$^{27}Al^+$quantum - logic clock with a systematic uncertainty below 10^{-18}," Phys. Rev. Lett. **123**, 033201 (2019).
12. T. Udem, J. Reichert, R. Holzwarth, *et al.*, "Absolute optical frequency measurement of the cesium D_1 line with a mode-locked laser," Phys. Rev. Lett. **82**, 3568–3571 (1999).
13. R. Holzwarth, A. Nevsky, M. Zimmermann, *et al.*, "Absolute frequency measurement of iodine lines with a femtosecond optical synthesizer," Appl. Phys. B **73**, 269–271 (2001).
14. M. J. Thorpe, K. D. Moll, R. J. Jones, *et al.*, "Broadband cavity ringdown spectroscopy for sensitive and rapid molecular detection," Science **311**, 1595–1599 (2006).
15. S. A. Diddams, L. Hollberg, and V. Mbele, "Molecular fingerprinting with the resolved modes of a femtosecond laser frequency comb," Nature **445**, 627–630 (2007).
16. C. Gohle, B. Stein, A. Schliesser, *et al.*, "Frequency comb Vernier spectroscopy for broadband, high-resolution, high-sensitivity absorption and dispersion spectra," Phys. Rev. Lett. **99**, 263902 (2007).
17. I. Coddington, W. C. Swann, and N. R. Newbury, "Coherent multiheterodyne spectroscopy using stabilized optical frequency combs," Phys. Rev. Lett. **100**, 013902 (2008).
18. N. Picqué and T. W. Hänsch, "Frequency comb spectroscopy," Nat. Photonics **13**, 146–157 (2019).
19. T. Steinmetz, T. Wilken, C. Araujo-Hauck, *et al.*, "Laser frequency combs for astronomical observations," Science **321**, 1335–1337 (2008).
20. C.-H. Li, A. J. Benedick, P. Fendel, *et al.*, "A laser frequency comb that enables radial velocity measurements with a precision of 1 cm s^{-1}," Nature **452**, 610–612 (2008).
21. B. R. Masters, P. T. C. So, C. Buehler, *et al.*, "Mitigating thermal mechanical damage potential during two-photon dermal imaging," J. Biomed. Opt. **9**, 1265–1270 (2004).
22. S. Hädrich, M. Krebs, A. Hoffmann, *et al.*, "Exploring new avenues in high repetition rate table-top coherent extreme ultraviolet sources," Light Sci. Appl. **4**, e320 (2015).
23. F. Köttig, D. Schade, J. R. Koehler, *et al.*, "Efficient single-cycle pulse compression of an ytterbium fiber laser at 10 MHz repetition rate," Opt. Express **28**, 9099–9110 (2020).
24. A. Cingöz, D. C. Yost, T. K. Allison, *et al.*, "Direct frequency comb spectroscopy in the extreme ultraviolet," Nature **482**, 68–71 (2012).
25. A. Schliesser, N. Picqué, and T. W. Hänsch, "Mid-infrared frequency combs," Nat. Photonics **6**, 440–449 (2012).
26. A. Ozawa and Y. Kobayashi, "VUV frequency-comb spectroscopy of atomic xenon," Phys. Rev. A **87**, 022507 (2013).
27. M. Herrmann, M. Haas, U. D. Jentschura, *et al.*, "Feasibility of coherent XUV spectroscopy on the 1S-2S transition in singly ionized helium," Phys. Rev. A **79**, 052505 (2009).

28. J. Moreno, F. Schmid, J. Weitenberg, *et al.*, "Toward XUV frequency comb spectroscopy of the 1 S-2 S transition in He^+," Eur. Phys. J. D **77**, 67 (2023).
29. L. S. Dreissen, C. Roth, E. L. Gründeman, *et al.*, "High-precision Ramsey-comb spectroscopy based on high-harmonic generation," Phys. Rev. Lett. **123**, 143001 (2019).
30. L. von der Wense and C. Zhang, "Concepts for direct frequency-comb spectroscopy of Th and an internal-conversion-based solid-state nuclear clock," Eur. Phys. J. D **74**, 146 (2020).
31. E. Peik, T. Schumm, M. S. Safronova, *et al.*, "Nuclear clocks for testing fundamental physics," Quantum Sci. Technol. **6**, 034002 (2021).
32. C. Zhang, P. Li, J. Jiang, *et al.*, "Tunable VUV frequency comb for ^{229m}Th nuclear spectroscopy," Opt. Lett. **47**, 5591–5594 (2022).
33. S. Kraemer, J. Moens, M. Athanasakis-Kaklamanakis, *et al.*, "Observation of the radiative decay of the ^{229}Th nuclear clock isomer," Nature **617**, 706–710 (2022).
34. C. Gohle, T. Udem, M. Herrmann, *et al.*, "A frequency comb in the extreme ultraviolet," Nature **436**, 234–237 (2005).
35. R. J. Jones, K. D. Moll, M. J. Thorpe, *et al.*, "Phase-coherent frequency combs in the vacuum ultraviolet via high-harmonic generation inside a femtosecond enhancement cavity," Phys. Rev. Lett. **94**, 193201 (2005).
36. A. Ozawa, J. Rauschenberger, C. Gohle, *et al.*, "High harmonic frequency combs for high resolution spectroscopy," Phys. Rev. Lett. **100**, 253901 (2008).
37. I. Pupeza, C. Zhang, M. Högner, *et al.*, "Extreme-ultraviolet frequency combs for precision metrology and attosecond science," Nat. Photonics **15**, 175–186 (2021).
38. J. Seres, E. Seres, C. Serrat, *et al.*, "All-solid-state VUV frequency comb at 160 nm using high-harmonic generation in nonlinear femtosecond enhancement cavity," Opt. Express **27**, 6618–6628 (2019).
39. H. Carstens, N. Lilienfein, S. Holzberger, *et al.*, "Megawatt-scale average-power ultrashort pulses in an enhancement cavity," Opt. Lett. **39**, 2595–2598 (2014).
40. S. Holzberger, N. Lilienfein, H. Carstens, *et al.*, "Femtosecond enhancement cavities in the nonlinear regime," Phys. Rev. Lett. **115**, 023902 (2015).
41. D. R. Carlson, J. Lee, J. Mongelli, *et al.*, "Intracavity ionization and pulse formation in femtosecond enhancement cavities," Opt. Lett. **36**, 2991–2993 (2011).
42. T. K. Allison, A. Cingöz, D. C. Yost, *et al.*, "Extreme nonlinear optics in a femtosecond enhancement cavity," Phys. Rev. Lett. **107**, 183903 (2011).
43. H. Wang, L. Amoudry, K. Cassou, *et al.*, "Prior-damage dynamics in a high-finesse optical enhancement cavity," Appl. Opt. **59**, 10995–11002 (2020).
44. A. Schliesser, C. Gohle, T. Udem, *et al.*, "Complete characterization of a broadband high-finesse cavity using an optical frequency comb," Opt. Express **14**, 5975–5983 (2006).
45. N. Lilienfein, C. Hofer, S. Holzberger, *et al.*, "Enhancement cavities for few-cycle pulses," Opt. Lett. **42**, 271–274 (2017).
46. F. Krausz and M. Ivanov, "Attosecond physics," Rev. Mod. Phys. **81**, 163–234 (2009).
47. G. Sansone, E. Benedetti, F. Calegari, *et al.*, "Isolated single-cycle attosecond pulses," Science **314**, 443–446 (2006).
48. O. Lundh, J. Lim, C. Rechatin, *et al.*, "Few femtosecond, few kiloampere electron bunch produced by a laser-plasma accelerator," Nat. Phys. **7**, 219–222 (2011).
49. A. J. Gonsalves, K. Nakamura, J. Daniels, *et al.*, "Petawatt laser guiding and electron beam acceleration to 8 GeV in a laser-heated capillary discharge waveguide," Phys. Rev. Lett. **122**, 084801 (2019).
50. D. Polli, P. Altoè, O. Weingart, *et al.*, "Conical intersection dynamics of the primary photoisomerization event in vision," Nature **467**, 440–443 (2010).
51. A. Baltuška, T. Udem, M. Uiberacker, *et al.*, "Attosecond control of electronic processes by intense light fields," Nature **421**, 611–615 (2003).
52. T. R. Schibli, J. Kim, O. Kuzucu, *et al.*, "Attosecond active synchronization of passively mode-locked lasers by balanced cross correlation," Opt. Lett. **28**, 947–949 (2003).
53. S.-W. Huang, G. Cirmi, J. Moses, *et al.*, "High-energy pulse synthesis with sub-cycle waveform control for strong-field physics," Nat. Photonics **5**, 475–479 (2011).
54. T. S. Khwaja and T. H. Yoon, "Phase-stable and selectable repetition-rate division of an optical frequency comb," Phys. Rev. A **102**, 043515 (2020).
55. T. Saule, S. Holzberger, O. De Vries, *et al.*, "Phase-stable, multi-μJ femtosecond pulses from a repetition-rate tunable Ti:Sa-oscillator-seeded Yb-fiber amplifier," Appl. Phys. B **123**, 17 (2017).
56. N. Ishii, K. Kaneshima, K. Kitano, *et al.*, "Carrier-envelope phase-dependent high harmonic generation in the water window using few-cycle infrared pulses," Nat. Commun. **5**, 3331 (2014).
57. O. de Vries, T. Saule, M. Plötner, *et al.*, "Acousto-optic pulse picking scheme with carrier-frequency-to-pulse-repetition-rate synchronization," Opt. Express **23**, 19586–19595 (2015).
58. F. Calegari, G. Sansone, S. Stagira, *et al.*, "Advances in attosecond science," J. Phys. B **49**, 062001 (2016).
59. F. Schmid, J. Moreno, J. Weitenberg, *et al.*, "An ultra-stable high-power optical frequency comb," APL Photonics (submitted for publication).
60. F. Schmid, J. Weitenberg, T. W. Hänsch, *et al.*, "Simple phase noise measurement scheme for cavity-stabilized laser systems," Opt. Lett. **44**, 2709–2712 (2019).
61. H. R. Carleton and W. T. Maloney, "A balanced optical heterodyne detector," Appl. Opt. **7**, 1241–1243 (1968).
62. K. Beil, S. T. Fredrich-Thornton, F. Tellkamp, *et al.*, "Thermal and laser properties of Yb:LuAG for kW thin disk lasers," Opt. Express **18**, 20712–20722 (2010).
63. M. Siebold, M. Loeser, F. Roeser, *et al.*, "High-energy, ceramic-disk Yb:LuAG laser amplifier," Opt. Express **20**, 21992–22000 (2012).
64. J. D. Deschênes and J. Genest, "Heterodyne beats between a continuous-wave laser and a frequency comb beyond the shot-noise limit of a single comb mode," Phys. Rev. A **87**, 023802 (2013).
65. J. Bechhoefer, "Feedback for physicists: a tutorial essay on control," Rev. Mod. Phys. **77**, 783–836 (2005).
66. A. Schönberg, H. S. Salman, A. Tajalli, *et al.*, "Below-threshold harmonic generation in gas-jets for th-229 nuclear spectroscopy," Opt. Express **31**, 12880–12893 (2023).
67. Y. Vidne, M. Rosenbluh, and T. W. Hansch, "Pulse picking by phase-coherent additive pulse generation in an external cavity," Opt. Lett. **28**, 2396–2398 (2003).
68. R. J. Jones and J. Ye, "High-repetition-rate coherent femtosecond pulse amplification with an external passive optical cavity," Opt. Lett. **29**, 2812–2814 (2004).